Heterogeneous Integration through Electrokinetic Migration

Electrical and Optical Addressing Techniques
Allow for More Rapid and Parallel Patterning
of Biological Species and Inorganic Objects

Mihrimah Ozkan[1], Cengiz S. Ozkan[2],
Osman Kibar[3], Mark M. Wang[3],
Sangeeta Bhatia[4], Sadik C. Esener[3]
[1]Electrical Engineering Department,
[2]Mechanical Engineering Department,
University of California at Riverside
[3]Electrical and Computer Engineering Dept.,
[4]Bioengineering Department,
University of California at San Diego

New technologies are continuously emerging from investigations at the interface of biology, engineering, physics, and chemistry. Recent advances have spanned many diverse applications, included drug delivery [1], novel schemes for lab-on-a-chip miniaturization, microfluidic networks [2, 3], DNA computing [4], self-assembly of mesoscopic objects [5], tissue engineering [6], and many more. In this study, we apply basic electrophoretic motion to semiconductor materials engineering for development of the next level of heterogeneous integration technology. Furthermore, we demonstrate the utility of these tools in integration of inorganic devices with biological species in order to explore the utility of these tools in biotechnological applications.

Several heterogeneous integration techniques currently available include flip-chip bonding [7, 8] and robotic pick-and-place processing for multichip integration [9,10] as well as probe force microscopy for handling smaller objects [11,12]. These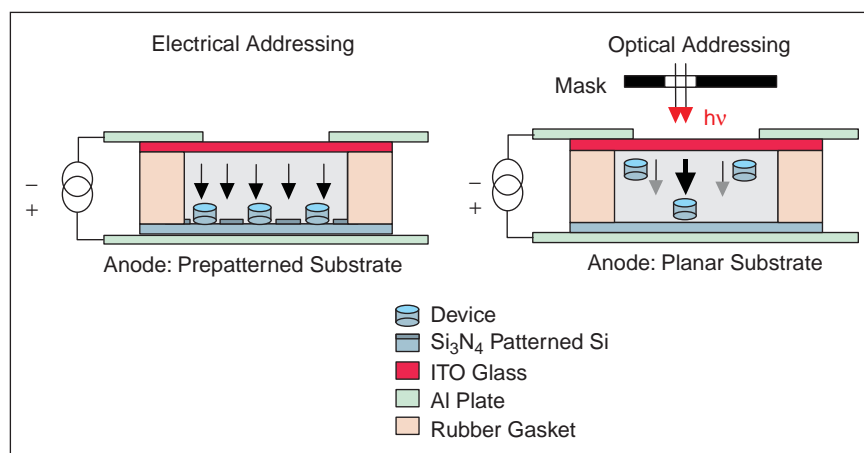 techniques do not allow the assembly of more than one type of component at a time and are very slow. In addition, they can handle only relatively large-size objects. Other heterogeneous integration methods being developed include fluidic self-assembly [13,14] and microelectrophoresis. Fluidic self-assembly sorts and positions objects based on their geometric shape, limiting its applicability. Microelectrophoresis is an electrochemical transport process based on the migration of charged particles in a suspension by the influence of an electric field. Important applications of this technique include the study of DNA/RNA hybridization and synthesis on bioelectronic chips [15,16]. An economically feasible heterogeneous integration technique needs to be developed to allow the rapid and parallel pick-and-place of individual devices to particular locations on a host substrate. In this article, we present a new class of pick-and-place heterogeneous integration processes based on *electrical field addressing* and/or *optical addressing* [17,18], which overcomes the limitations of other techniques. The primary advantage in these techniques is *parallelism*, which minimizes the time and cost involved in the pick-and-place patterning process.

Theory

In an electrochemical cell, electrolytic conduction occurs by the movement of charge carriers to their respective opposite terminals. The basic principle of our pick-and-place assembly technique depends on the movement of the charged species and ions to oppositely charged electrodes within an electrolyte solution [17, 18]. In a parallel electrode system as we have used, the electric field is perpendicular to the electrodes. The ions or molecules move along the electric field between the electrodes. Lateral migration of species appears to be the result of electrohydrodynamic effects, wherein gradients in current density, caused by the presence of particles or inhomogeneities near the electrode surface, generate localized fluid flow [19, 20].

In the following sections, a new approach for analysis of an electrochemical system will be described. In this analysis, well-known solid-state band energy distribution phenomenon for VLSI devices will be applied to our electrochemical system, which includes liquid-solid junctions.

1. A schematic illustration of the experimental setup.

Electrical Addressing

Optical Addressing

Mask

hv

$-$ $+$ Anode: Prepatterned Substrate

$-$ $+$ Anode: Planar Substrate

Device
Si_3N_4 Patterned Si
ITO Glass
Al Plate
Rubber Gasket

Electrolytic Cell

Figure 1 illustrates a schematic of the electrochemical cell setup used. This cell is formed by a top indium tin oxide (ITO)-coated glass plate, and a bottom wide area n-n$^+$ planar junction diode, spaced by a rubber gasket. The transparent container is clamped between aluminum (Al) plates, and contact to the Al plates via cables to a power supply completes the circuit. In this setup, the electric field is perpendicular to the surface of the substrate and parallel to the gravitational force. The substrate, which will be used as a host during the integration process, can be chosen from a different material. The counter electrode (ITO) is selected such that it will allow visual observations during experimentation.

System Analysis

The current versus voltage (I-V) behavior of this system is shown in Fig. 2, resembling that of a diode except for two critical (threshold) potentials that must be exceeded for current to flow [21-24]. The two critical potentials result from the potential drops at the liquid-solid interfaces at both electrodes. In this section, a new approach, which is commonly used for solid-state device analysis, will be used to analyze the potential drop at the liquid-solid interface.

To understand the operation of the optoelectrochemical circuit, we first consider a circuit under conditions of no illumination and no applied bias. At one electrode, there is contact between an n-type semiconductor and a solution containing molecules H$^+$ and OH$^-$, capable of undergoing a redox (reduction/oxidation) reaction. In an aqueous solution there are several possible sets of redox reactions that can occur, depending upon the pH of the solution. In solutions that are of approximately neutral pH, such as those we use in our electrochemical circuits (de-ionized water), the oxidation of the water at the anode produces oxygen (O$_2$) and aqueous hydrogen ions, whereas the reduction of aqueous hydrogen ions at the cathode generates molecular hydrogen [21]. Since we are interested in single electron and single hole transfer at the solid-liquid interface, in this article we will use an unconventional redox reaction for the electrolysis of pure water. Gurney [25] used the same approach in HCl-H$_2$0 system analysis.
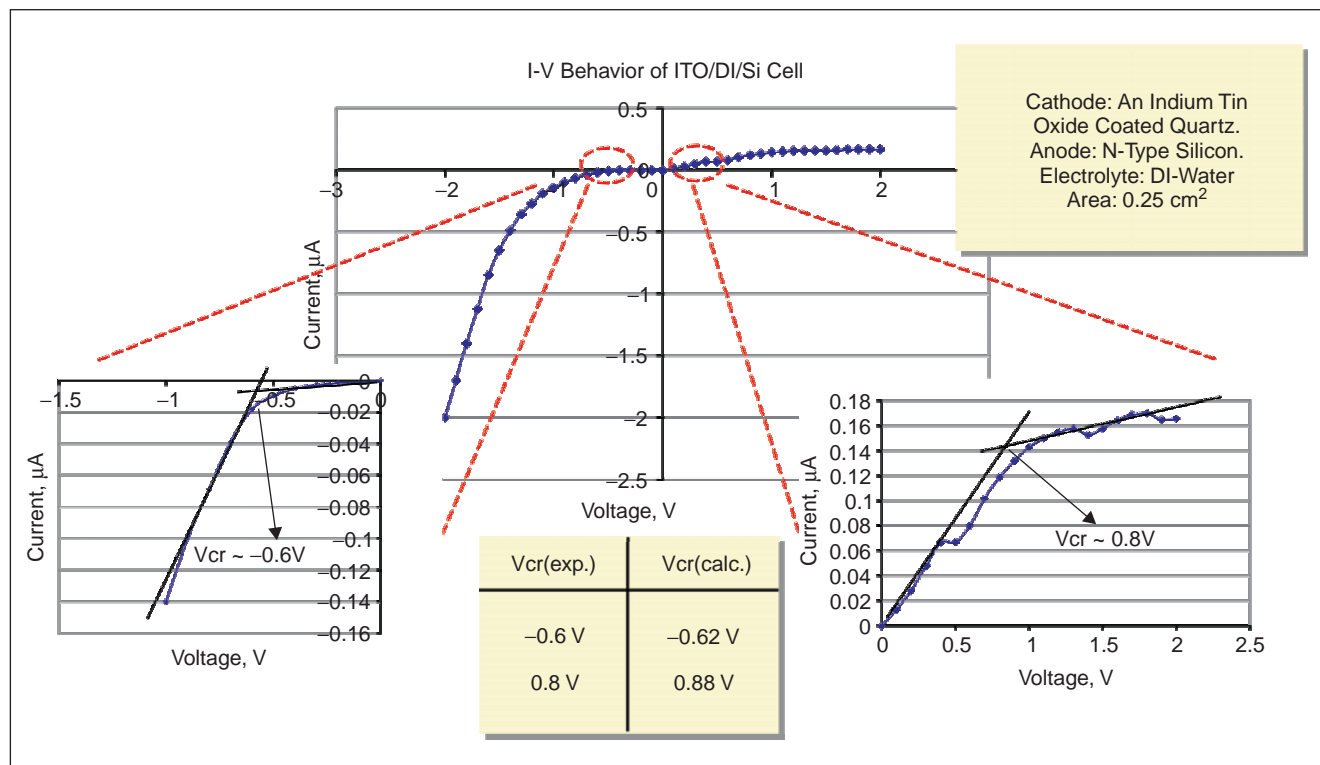
Anodic reaction:

$$(OH - H_2O)^- + h^+ \rightarrow (OH - H_2O) \quad (1)$$
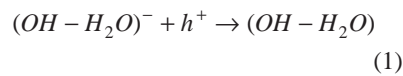
Cathodic reaction:

$$(H - H_2O)^+ + e^- \rightarrow H - H_2O. \quad (2)$$
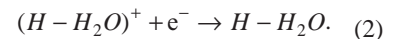
Equation (1) shows the anodic oxidation of OH$^-$ ions and Eq. (2) represents the

> **The electrical-addressing system described earlier is useful for applications in which a large number of identical devices are to be placed in a uniform array.**

I-V Behavior of ITO/DI/Si Cell

Cathode: An Indium Tin Oxide Coated Quartz.
Anode: N-Type Silicon.
Electrolyte: DI-Water
Area: 0.25 cm^2

Vcr ~ −0.6V

Vcr ~ 0.8V

Vcr(exp.)	Vcr(calc.)
−0.6 V	−0.62 V
0.8 V	0.88 V

2. Measured current-voltage characteristics of the ITO-deionized water-Si cell. Calculated and measured V$_{cr}$ values are in good agreement.

cathodic reduction of aqueous hydrogen ions. A locally basic environment arises at the cathode, while a locally acidic environment arises at the anode. At the electrodes, the ionic conduction is converted into electronic conduction by the aid of redox reactions.

At the interface of any liquid and semiconductor materials, differences in electrostatic potential cause electron movement. Specifically, if the electrochemical potential of the isolated semiconductor (n-Si) is more negative than the electrochemical potential of the isolated solution phase, elec-

trons move from the semiconductor to the acceptor ions in the solution. The transfer of electrons across the semiconductor-liquid junction disrupts the original charge neutrality of the semiconductor and of the solution. This interfacial charge transfer introduces an electron-depleted region in the semiconductor. The difference of electrostatic potential between a semiconductor and a liquid forms an electric double layer at the interface [26]. This layer includes three distinct sublayers: 1) a diffuse charge layer in the ionic solution (Gouy Layer), 2) a compact layer of adsorbed water molecules (Helmholtz Layer), and 3) a diffuse charge layer in the semiconductor (space charge layer). The potential difference between the semiconductor and the liquid is the sum of the potential drops at these three individual sublayers, as given below:

Total Charge:

$$\Delta\Phi_{\text{total}} = \Delta\Phi_{SC} + \Delta\Phi_H + \Delta\Phi_{\text{DIFF}}. \quad (3)$$

Figure 3 illustrates the distribution of these layers at the liquid-semiconductor interface.

Pleskov et al. [27] and Batchelor et al. [28] have shown that, if: a) the semiconductor has a low surface state concentration, b) the semiconductor is minimally doped, and c) ionic concentration of the solution is $> 10^{-2}$M, then the potential drop at the Gouy diffuse layer within the liquid can be neglected. For the work presented in this article, we have carried out our experiments with these assumptions, where the total potential drop at the liquid-semiconductor junction is equal to $\Delta\Phi_{SC} + \Delta\Phi_H$. In order to calculate this potential, we first need to estimate the

Fermi level of the liquid. To this end, we used an experimental setup, where the host substrate is silicon, the liquid is pure water, and the counter electrode is ITO (indium tin oxide). We measured the potential drop at the liquid-semiconductor interface by using a commercial potentiostat with respect to a saturated calomel electrode (SCE). Since the potential of the reference electrode is known (4.74 V with respect to vacuum), we could calculate the potential drop between the liquid and the semiconductor using the following equation [29]:

$$V_M + V_{\text{REF}} = \Delta\Phi_{SC/L} - q\varepsilon_f^{SC} \quad (4)$$
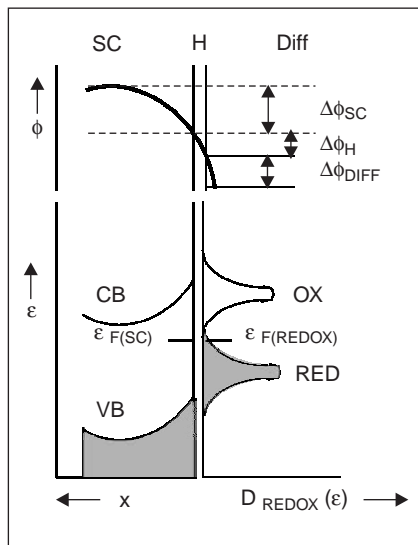
where:

V_M = measured potential of the cell (0.37 V in our experiment);

V_{REF} = reference electrode (SCE) potential (4.74 V with respect to vacuum);

$\Delta\Phi_{SC/L}$ = potential drop at the semiconductor-liquid interface; and

ε_f^{SC} = Fermi level of the semiconductor.

The Fermi level of the silicon electrode we used, $\varepsilon_f^{SC} = -4.32$ eV (with respect to vacuum), is known based on its doping concentration (10^{16}/cm^3). By calculating the potential drop at the semiconductor-liquid interface (0.79 V), we obtain a functional estimate of the Fermi level of water in our experiment as 5.115 eV. The reader should note the lack of true "Fermi level" phenomenon for liquids. However, in order to predict junction behavior, we assume that the "Fermi level" can be approximated at this constant value. Thus, we can now use our experimental set-up to determine the Fermi level of the actual liquids we use during our pick-and-place experiments. Initially, we used de-ionized

3. Schematic illustration of the band-bending formation at the semiconductor-liquid interface where both semiconductor and liquid are in equilibrium. Three potential regions make up the electrical double layer at the interface: Space charge region at the semiconductor (SC), Helmholtz layer (H), and Diffuse or Gouy-Chapman layer (DIFF).
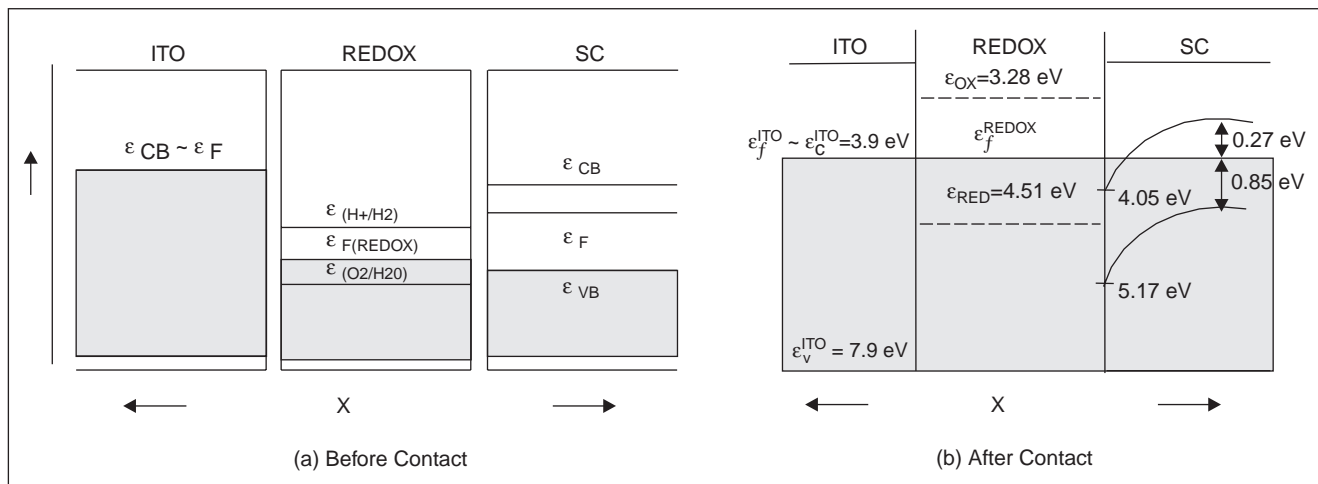
4. Energy-level diagram of the ITO-liquid-semiconductor electrochemical cell system just before contact, and at equilibrium right after contact. All energy levels are referenced to vacuum level.

water as an electrolyte solution and, since water is polar [30], it can be assumed that the Fermi level of water is at the mid-point of the reduction, $E_{(RED)}$, and oxidation, $E_{(OX)}$, reaction energies. Since the OH^- and H^+ ions in water split at 1.23 V (with respect to a hydrogen electrode), ±0.615 V are the $E_{(OX)}$ and $E_{(RED)}$ levels in water, respectively. The following energy diagram (Fig. 4) can then be constructed from the calculated values and known material properties of ITO and silicon. Figure 4 gives the band energy distribution of ITO-liquid-silicon just before contact and immediately after contact. The Fermi levels equalize after all the layers make contact. As a result, potential drops result at the interfaces to accommodate the potential differences between the regions. At equilibrium, the silicon substrate accumulates electrons at the surface. The flat band potential for silicon is calculated as ~ 0.42 eV from Fig. 4. This result is found to be similar to the measured flat band potential shown in Fig. 2.

From the energy diagram in Fig. 4, we calculated the potential barriers for electron flow at the ITO-liquid and SC-liquid interfaces. This model predicts critical voltage levels (V_{cr}) at which the current will start flowing through the system. The values can be predicted by using Eq. (3) and Fig. 4. The calculated values (−0.62 V, 0.88 V) are confirmed with experimental values (−0.6 V, 0.8 V). Figure 2 shows the measured current-voltage characteristic of this system along with the calculated and measured V_{cr} values.

A semiconductor device simulation tool (SEDAN, Stanford University, Stanford, CA) was used to predict the current and voltage behavior of the water-silicon interface. This junction is a depleted Schottky diode that forms at the liquid-semiconductor interface. The results of this simulation are given in Fig. 5. The SEDAN-simulated current-voltage results are in a good agreement with the experimental results. This result shows that water-silicon junction properties dominate and determine the overall system behavior. This result is important and can be used to improve the system performance further by tailoring the water-silicon interface only.
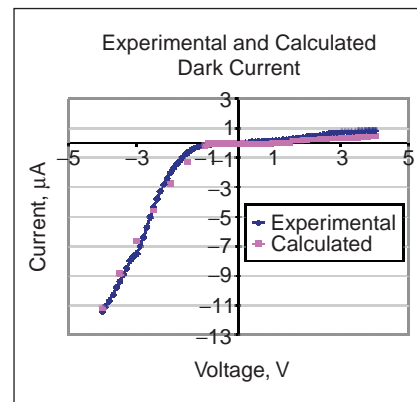
After completion of the analyses of the system in Fig. 1 under applied bias conditions, photon-induced conductivity can also be predicted. In our experiments, we used a semiconductor-liquid (silicon-pure water) junction under illumination. Absorption of photons in the n-type semicon-ductor creates electrons and holes, giving rise to both minority and majority carrier photo-induced currents. The majority carrier current changes a negligible amount under illumination. However, there is an appreciable change in the minority carrier current. The total current with illumination is given by the standard equation for a diode [31]:

$$I_{total} =$$
$$I_{ph}(V_a) - I_o\left[\exp\left(-\frac{q(V_a - V_{th})}{kT}\right) - 1\right].$$
(5)

The parameter I_o is the reverse constant current, V_a is applied voltage, V_{th} is the threshold voltage required for the current flow, and T is the ambient temperature in °K. The photo-generated minority carrier current I_{ph} is equal to the photon flux absorbed by the semiconductor multiplied by the area that is illuminated, and by the electron charge q.

In these calculations, it was assumed that there are no surface states, which would complicate the band diagrams and the analysis of the current flow. Figure 6 illustrates the measured I-V characteristics of the ITO-deionized water-Si cell in the dark and with illumination of 2.5 mW laser power (a semiconductor laser with 680-nm wavelength was used). In this graph, the calculated photocurrent by using Eq. (5) is also shown. The photo-induced current is higher at the positive applied bias regime because of the photo-generated carriers. When an electron-hole pair is generated in the space charge region in silicon by photon absorption, electrons lower their energy and move into the bulk of the semiconductor. On the other hand, holes generated will move toward the silicon surface and be involved in redox reactions.

> **Applications of the electrical patterning process include all platforms that require parallel access to immobilized cells.**

This phenomenon will increase the charge transfer rate between silicon and liquid as well as increase the current density of the system. At the negative bias regime, the opposite behavior is observed. The photo-induced current is lower than the dark current. This behavior can be explained by photo-enhanced ion or molecule absorption at the silicon surface. Due to the enhanced absorption, extra positive charge will be present at the liquid side of the interface, which is not balanced by charges at the electron-accumulating silicon surface [21, 25]. Therefore, negatively charged ions or molecules inside the liquid will move near to the interface in order to balance the extra charge generated by absorption of ions or molecules to the surface. This migration will disturb the balanced cathodic behavior and will generate local anodic reactions as well. As a result, the overall cathodic current will be reduced under illumination.
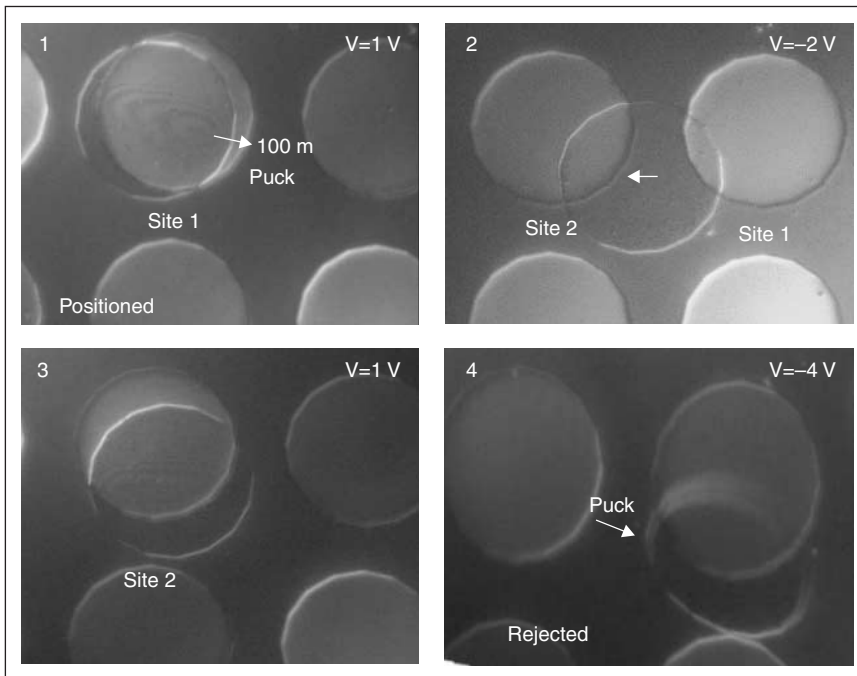

5. Comparison of the SEDAN simulation results with the measured current-voltage values.
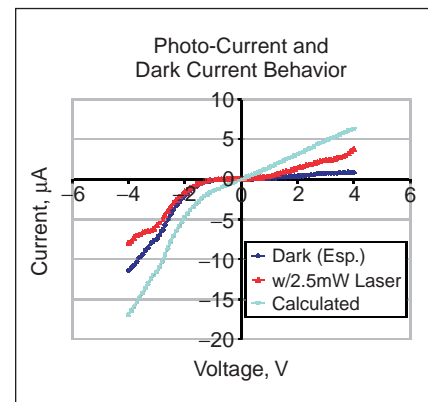
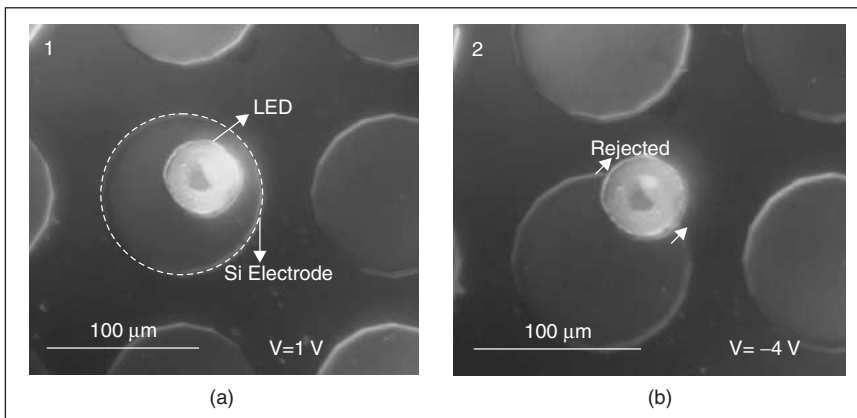**6. Comparison of the photo-induced current-voltage behavior with theoretical calculation and measured dark current.**
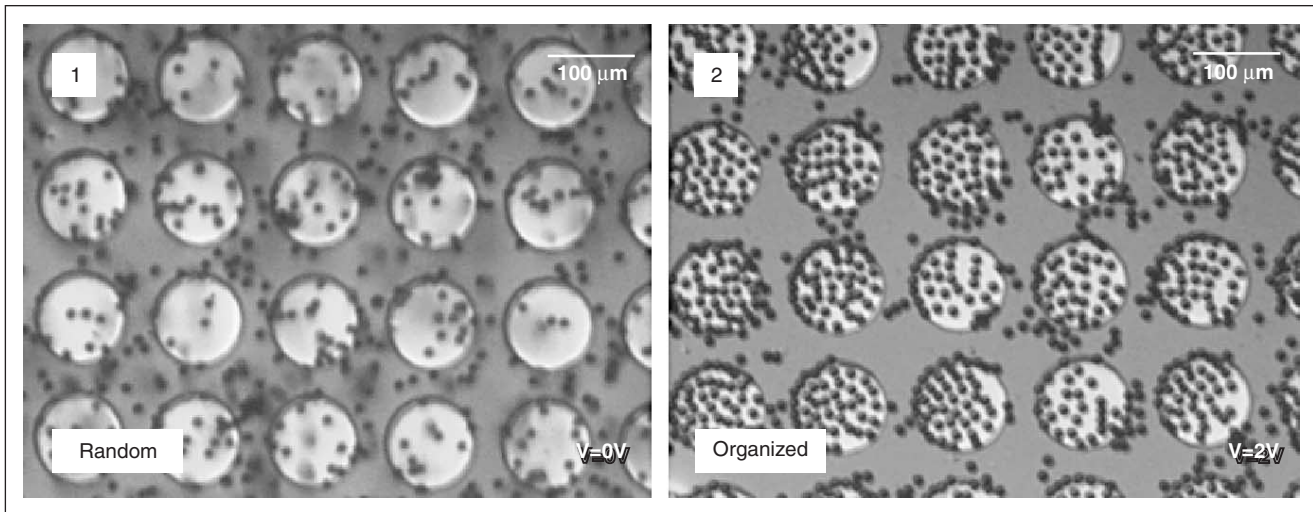
7. 10-μm polystyrene beads are positioned with applied bias of 2.0 V.

8. 100-μm SiO2 puck is picked and placed by an applied bias of 2 V. The puck is moved to the next neighbor electrode and rejected from Site 2 by an applied bias of –4V.

9. (a) Placement of the 50-μm diameter LED by applied reverse bias on the silicon electrode. (b) Rejection of an LED by application of a forward bias.

The photo-current calculated by using Eq. (5) gives an electrical behavior as expected. The photocurrent in the positive bias regime was higher than the dark current, which is also in very good agreement with measured values. But the calculated current values are much higher than the experimental results. This is because Eq. (5) does not include the photon loss due to scattering or reflection at the ITO-silicon interface and inside the liquid. Since the equation does not include the photon loss factor for the whole system, the calculated current is higher than expected. Similar behavior is also valid in the negative bias region.

Experimental Results

Electrical Addressing

For pick-and-place patterning via electrical addressing, the bottom planar diode was replaced with a patterned array of silicon electrodes. To fabricate this array, a layer of Si_3N_4 was deposited using plasma-enhanced chemical vapor deposition on an n-type silicon substrate, which was subsequently patterned to fabricate 100-μm diameter circular openings where the silicon surface was exposed. In this manner, charged species can be localized over the surface of each circular electrode. Figure 7 shows results of an experiment where the spatial positions of negatively charged beads are presented as a function of the applied bias voltage. Randomly distributed beads from the solution rapidly localize (~3 s) over the circular openings when a positive bias of 2.0 V is applied to the silicon substrate. When a bias voltage of −2.0 volts is applied, beads move away from the silicon electrode regions towards the neutral (nitride) regions of the substrate

due to Coulomb repulsion. The positioning mechanism involves processes such as simple Coulomb interactions, which bring particles close to the electrodes, and electrohydrodynamic and electroosmotic effects that determine the lateral migration of the beads. In the absence of the applied bias, beads arrive at the surface by sedimentation. Once the particles arrive at the surface, electro-osmotic flow of the liquid around the beads occurs. Liquid will flow upward along the particle surface, being transported towards the particle along the electrode surface [19].

Electrical addressing was then applied to pick and place larger objects, including micromachined components such as cylindrical SiO_2 test pucks (passive devices) and active devices including light-emitting diodes. Both viscous drag and inertial forces would be larger in this case as predicted by Hiemenz [32]. These objects first were charged by immersion in a sodium dodecyl sulfate solution. For example, Fig. 8 describes the pick-and-place assembly of a 100-μm diameter and 0.65-mm thick SiO_2 puck on a similar substrate. Upon applying a bias of 1.0 V, the test puck was localized to Site 1, as shown in the first frame. When the bias voltage was reversed (−2.0 V), the puck was repelled from Site 1, as shown in the second frame. Under negative bias conditions, the puck moved laterally by electro-osmotic and electrohydrodynamic forces. When it approached the next neighbor electrode (Site 2), the applied bias was reversed again, and the puck was attracted to this new location. At this new location, at applied bias of − 4V, the puck was rejected from the surface.

A similar experiment was conducted with 50-μm diameter SiO_2 pucks [17,18]. The required bias voltage for rejecting 100-μm pucks from the surface was higher (−4.0 V) than for the 50-μm puck case. This voltage correlates well with the expected increase in attractive forces due to van der Waals forces over a larger surface area and a similar charge density, when compared to smaller pucks. The van der Waals attraction of the larger puck to the surface was stronger due to its larger surface area, requiring a larger potential to reject it from the surface of the electrode. The velocity of larger objects also differed from smaller ones, as expected. Object velocity should increase, due solely to charge effects, but it decreases due to increase inertial and viscous forces. Qualitatively, we observed that larger objects of

a similar shape have a relatively slower velocity, suggesting that charge effects dominate their behavior.

To demonstrate the pick-and-place patterning of active devices, a 50-μm diameter light-emitting diode was used. Figure 9 summarizes the results of this experiment, where spatial position is presented as a function of the bias voltage. Once in place, the LED could be fusion bonded and externally controlled.

Next, we have used the same technique for patterning biological species including DNA molecules and live mammalian cells [17]. Figure 10(a) and (b) summarizes the patterning process of mammalian cells from human (fibrosarcoma) and mouse (fibroblasts), respectively. Mammalian cells are typically negatively charged due to the numerous sialic acid residues present in the glycocalyx. Thus, cells behave as negatively charged particles in an electrolytic conducting medium. However, a major difference in this experiment from the previous ones stems from the composition of the electrolytic solution. Cells require osmotic equilibrium (300 mOsm) to retain cell shape and viability. Therefore, deionized water cannot be used as a low-conductance buffer. Instead, we have adjusted the solution for osmolarity and nutrients. Hence, as
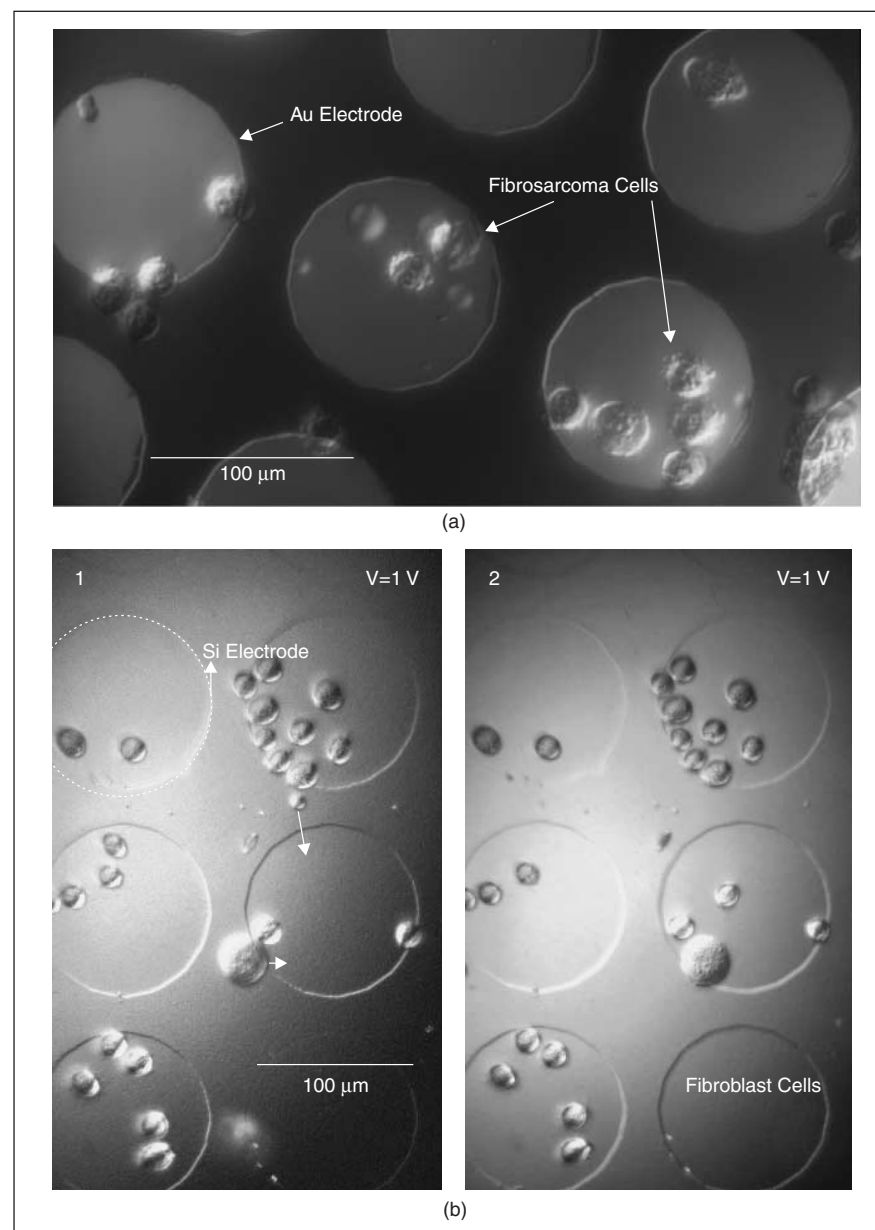
10. (a) Human fibrosarcoma cells (20-30-μm diameter) are patterned on the substrate. (b) Mouse fibroblast cells are patterned on silicon electrode under applied bias.
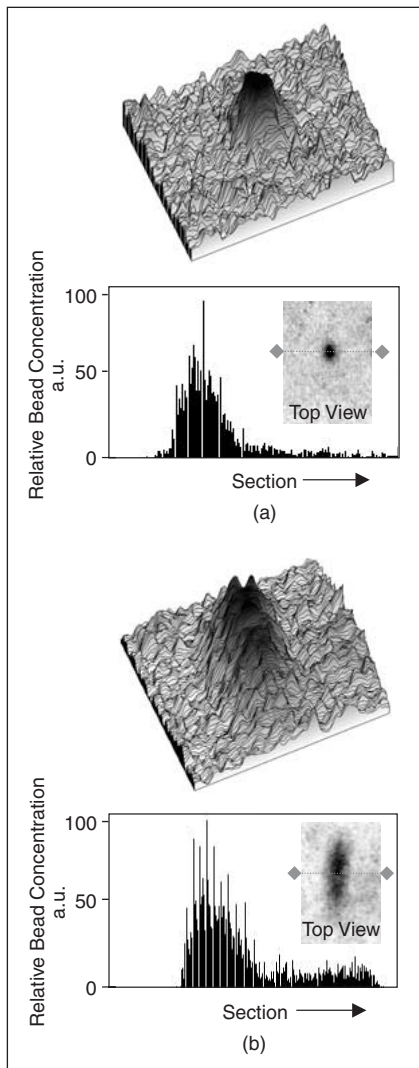
11. Highly concentrated beads formed using a mask during illumination. 3-D graph represents the bead distribution across the sample and the x-y graph represents the relative bead concentration across the section-line on the picture: (a) with a circular mask; (b) with an elliptical mask.

shown in Fig. 10(a), negatively charged human cells could be attracted to the gold-patterned silicon surface of 100-μm diameter. Preliminary data suggest that cells remain viable for 24 hours under these conditions. More than 90% of the cells were positioned over the electrodes, while the remainder of the cells were positioned over the neutral regions, because of electrostatic interaction between cells and substrate. We will address this issue in future experiments with strategies to determine adhesion of cells that fall under a gravitational field.

The electrical-addressing system described earlier is useful for applications in which a large number of identical devices are to be placed in a uniform array. The backside of the substrate can also be patterned with electrical contacts so that various locations on the substrate can be addressed individually for selective patterning [15]. It has been shown previously that high-voltage biasing during the patterning process should be avoided due to production of H_2O_2 during electrolysis. Currently, experiments are underway to quantify cell viability with vital fluorescent dyes and to quantify cell function by tracking cell division and morphology. Nevertheless, the results presented here demonstrate both biological species and inorganic objects. Applications of this patterning process include all platforms that require parallel access to immobilized cells including: cell-based biosensing, cell-based drug discovery, and high-throughput phenotyping.

Optical Addressing

Optoelectronic addressing adds a supplementary degree of freedom. Charged devices or objects within the electrochemical solution are attracted to illuminated regions on a photoconductive substrate due to a potential drop resulting from absorption of photons (Fig. 1). Absorption of photons in the n-type semiconductor creates electrons and holes, giving rise to both minority and majority carrier photo-induced currents. Figure 6 illustrates this effect on the current versus voltage behavior. Thus, the illuminated region becomes a temporary electrode, without requiring microfabricated patterning.

To demonstrate optical addressing, negatively charged polystyrene beads (0.87-μm diameter) were suspended in deionized water in the electrochemical cell. Initially, the beads were randomly distributed over the substrate surface. A reverse bias of 2.0 V was applied across the cell, and a He-Ne laser ($\lambda = 632$ nm) was used to illuminate a small area on the silicon substrate. In this illuminated region, the generated photocurrent attracted the negatively charged beads towards the substrate. Images in Fig. 11(a) and (b) illustrate the fluorescence obtained from highly concentrated bead areas for two different experiments, where elliptic and circular slits were used during initial laser radiation. In this figure, the amount of fluorescence is shown in graphical form. Relative concentration of the beads in the illuminated and dark regions gives very high ratio of approximately 80 to 1. Thus, electrode shape and size can be modified dynamically through modulation of incident light. Finally, when optical and electrical addressing are combined, several different types of optoelectronic devices can be picked and placed on the same substrate at the same time, allowing an efficient fabrication scheme for complex arrays of devices and objects of both inorganic and organic origins.

Mihrimah Ozkan is a Ph.D. student in the Electrical and Computer Engineering Department at the University of California at San Diego. She received her M.S. degree in materials science and Engineering from Stanford University. She is currently working on electrokinetic and optical patterning of optoelectronic devices and biological species. She has been awarded the Graduate Student Award at the Materials Research Society (1999), Biomedical Engineering Society (2000) and Jacobs School of Engineering (2001) for her academic and research achievements. She holds a number of pending patents on bio-electrical engineering interface.

C.S. Ozkan received his Ph.D. and M.S. degrees in materials science and Engineering from Stanford University in 1997. He is currently a senior development engineer at Applied Micro Circuits Corporation where he is working on SiGe bipolar device technologies. He is also a Visiting Scientist and a Lecturer to the Electrical Engineering Department at the University of California at San Diego. His research interests are biofluidics, nanotechnology, and microelectromechanical systems. Dr. Ozkan is holding several pending patents.

Osman Kibar received his Ph.D. and M.S. degrees in applied physics and electrical engineering from the University of California at San Diego in 1999 and in 1995, respectively. He is currently a research associate in the same department. His current research interests are semiconductor

device physics, optoelectronic devices, laser physics, and projects involved with biophotonics and X-ray spectroscopy. Dr. Kibar is holding several pending patents.

Mark M. Wang received his B.S. in physics from Stanford University in 1994 and received his Ph.D. in electrical engineering from the University of California at San Diego in 1999 while working in the field of three-dimensional optical memories. Currently he is a postdoctoral researcher at UCSD working on the integration of optoelectronic devices into optical interconnection and biophotonic systems.

Sangeeta Bhatia graduated from the Massachusetts Institute of Technology with an M.S. in mechanical engineering, a Ph.D. in bioengineering, and from Harvard Medical School with a medical doctorate. She has also worked in pharmaceutical drug development at ICI Pharmaceuticals and in medical device design at Pfizer Hospital Products. She is now an assistant professor of bioengineering and medicine at UCSD and the director of the Microscale Tissue Engineering Laboratory. Her research interests are in tissue engineering of the liver and the development of enabling biological technologies from microelectromechanical tools.

Sadik C. Esener received the Ph.D. degree in applied physics and electrical engineering from the University of California at San Diego in 1987. He joined the ECE faculty in 1987, became an associate professor in 1991 and a full professor in 1996. He is currently leading the Optoelectronic Computing Group and directing the Opto-Electronic Stacked Processors industry/university consortium as well as the Fast Read-out Optical Storage consortium funded by DARPA. He received a certificate of recognition from NASA in March 1987 for his work on optically addressed RAM. Prof. Esener has written four book chapters, published more than 80 research articles in refereed journals, presented numerous papers in scientific meetings, and holds four patents. Esener is also a cofounder of three local companies and president of Call/Recall Inc.

Address for Correspondence: Mihrimah Ozkan, Electrical Engineering Dept., University of California at Riverside, Riverside, California. E-mail: mihrimah@ece.ucsd.edu.

References

[1] R.F. Service, "Silicon chips find role as in vivo pharmacist," *Science*, vol. 283, pp. 619, Jan. 29, 1999.

[2] R.B.M. Schasfoort, S. Schautmann, J. Hendrikse, and A. vab den Berg, "Field effect flow control for microfabricated fluidic networks," *Science*, vol. 286, pp. 942-945, Oct. 20, 1999.

[3] D.J. Harrison, K. Fluri, K. Seiler, Z. Fan, C.S. Effenhauser, and A. Monz, *Science*, vol. 261, p. 895, 1993.

[4] P.W.K. Rothemund, "Using lateral capillary forces to compute by self-assembly," *Science*, vol. 97, no. 3, Feb. 1, 2000.

[5] T.L. Breen, J. Tien, S.R.J. Oliver, T. Hadzic, and G.M. Whitesides, "Design and self-assembly of open, regular, 3D mesostructures," *Science*, vol. 284, pp. 948-951, May 7,1999.

[6] S.N. Bhatia, *Microfabrication in Tissue Engineering and Bioartificial Organs,* S. Senturia, Ed. Norwell, MA: Kluwer, 1999.

[7] M. Klein, H. Oppermann, R. Kalicki, R. Aschenbrenner, and H. Reichl, "Single chip bumping and reliability for flip chip processes," *Microelectronics Reliability*, vol. 39, no. 9, pp. 1389-1397, Sept. 1999.

[8] T.A. Nguty and N.N. Ekere, "Chip scale vs. flip chip: Issues to consider," *Circuits Assembly*, vol. 10, no. 11, pp. 26-32, Nov. 1999.

[9] E. Doskocz, Y. Shtessel, and C. Katsinis, "MIMO sliding mode control of a robotic 'pick and place' system modeled as an inverted pendulum on a moving cart," in *Proc. 13th Southeastern Symp. Syst. Theory*, Morgantown, WV, Mar. 8-10, 1998, pp. 379-383.

[10] J.F. Mack, "Getting started on pick-and-place robots," in *Hydraulics and Pneumatics*, vol. 50, no. 11. Cleveland, OH: Penton, Nov. 1997, pp. 43-44.

[11] D.M. Taylor, "Molecular nanostructures and their electrical probing," *Thin Solid Films*, vol. 331, no. 1-2, Oct. 15, 1998.

[12] P. Cyganik, P. Korecki, J. Szymonska, M. Szymonski, and Z. Postawa, "Scanning probe microscopy of self-assembled organic monolayers," *Electron Technol.*, vol. 31, no. 3-4, pp. 440-446, 1998.

[13] J.J. Talghader, "Integration of LEDs and VCSELs using fluidic self-assembly," in *Proc. SPIE—The International Society for Optical Engineering*, vol. 3286. San Jose, CA: Vertical-Cavity Surface-Emitting Lasers II, 28-29 Jan. 1998, pp. 86-95.

[14] H.J.J. Yeh and J.S. Smith, "Fluidic self-assembly for the integration of GaAs LED on Si substrates," *IEEE Photonics Lett.*, vol. 6, no. 6, June 1994.

[15] J. Cheng, E.L. Sheldon, L.Wu, A. Uribe, L.O. Gerrue, J. Carrino, M.J. Heller, and J.P. O'Connell, "Preparation and hybridization analysis of DNA/RNA from E. coli on microfabricated bioelectronic chips," *Nature*, vol. 16, no. 6, pp. 541-546, June 1998.

[16] C. Edman, D.E. Raymond, D.J. Wu, E. Tu, R.G. Sosnowski, W.F. Butler, M. Nerenberg, and M.J. Heller, "Electrical field directed nucleic acid hybridization on microchips," *NucleicAcids Res.*, vol. 25, no. 24, pp. 4907-4914, 1997.

[17] M. Ozkan, D. Hartmann, C.S. Ozkan, E. Tu, S. Bhatia, M. Heller, and S.C. Esener, "A new electrochemical system for pick and place of devices and biological cells on a silicon substrate," presented at the *Symp. G, 1999 Fall Meeting of the Materials Research Society*, Boston, MA.

[18] M. Ozkan, O. Kibar, C. S. Ozkan, and S.C. Esener, "A new optical and electric-field assisted fluidic technique for pick and place of electronic devices," presented at *OC 2000*, Canada.

[19] Y. Solomentsev, M. Bohmer, and J.L. Anderson, "Particle clustering and pattern formation during electrophoretic deposition: A hydrodynamic model," *Langmuir,* vol. 13, pp. 6058-6068, 1997.

[20] M. Trau, D.A. Saville, and I.A. Aksay, "Field-induced layering of colloidal crystals," *Science*, vol. 272, pp. 706-709, 1996.

[21] N. Sato, *Electrochemistry at Metal and Semiconductor Electrodes*. New York: Elsevier, 1998.

[22] W. Jaegermann, "The semiconductor/electrolyte interface: A surface science approach," *Modern Aspects of Electrochemistry*, no. 30. New York: Plenum, 1996.

[23] M.X. Tan, P.E. Laibinis, S.T. Nguyen, J.M. Kesselman, C.E. Stanton, and N.S. Leweis, "Principles and applications of semiconductor photoelectrochemistry," in *Progress in Inorganic Chemistry*, vol. 41. New York: Wiley, 1994.

[24] S.R. Morrison, *Electrochemistry at Semiconductor and Oxidized Metal Electrodes*. New York: Plenum, 1980.

[25] R.W. Gurney, *Proc. R. Soc. Lond. A,* pp. 134-137, 1932.

[26] Y.V. Pleskov, *Electric Double Layer on Semiconductor Electrodes*, P.N. Bartlett, Ed. New York: Plenum, 1980.

[27] M.D. Krotova and Yu. V. Pleskov, "Relationships governing photoelectric emission of electrons from a semiconductor into a polar medium," *Fizika Tverdogo Tela*, vol. 15, no. 9, pp. 806-808, Sept. 1973.

[28] R.A. Batchelor and A. Hamnett, *Surface States on Semiconductors*, J.O. Bockris, Ed. New York: Plenum, 1992.

[29] J.O.M. Bockris and S.U.M. Khan, *Surface Electrochemistry: A Molecular Level Approach*. New York: Plenum, 1993.

[30] H. Gerischer, *Advance in Electrochemistry and Electrochemical Engineering*. New York: Wiley, 1961.

[31] Y.V. Pleskov, *Semiconductor Photoelectrochemistry*. New York: Consultants Bureau, 1986.

[32] P.C. Hiemenz, *Principles of Colloid and Surface Chemistry*. New York: Marcel Dekker, 1986.